

Research Article

Open Access



# BaTiO<sub>3</sub>-NaNbO<sub>3</sub> energy storage ceramics with an ultrafast charge-discharge rate and temperature-stable power density

Peiyao Zhao, Longtu Li, Xiaohui Wang

State Key Laboratory of New Ceramics and Fine Processing, School of Materials Science and Engineering, Tsinghua University, Beijing 100084, China.

**Correspondence to:** Prof. Xiaohui Wang, State Key Laboratory of New Ceramics and Fine Processing, School of Materials Science and Engineering, Tsinghua University, Beijing 100084, China. E-mail: wxh@tsinghua.edu.cn

**How to cite this article:** Zhao P, Li L, Wang X. BaTiO<sub>3</sub>-NaNbO<sub>3</sub> energy storage ceramics with an ultrafast charge-discharge rate and temperature-stable power density. *Microstructures* 2023;3:2023002. <https://dx.doi.org/10.20517/microstructures.2022.21>

**Received:** 26 Aug 2022 **First Decision:** 28 Sep 2022 **Revised:** 11 Oct 2022 **Accepted:** 28 Oct 2022 **Published:** 5 Jan 2023

**Academic Editors:** Shiqing Deng, Ruzhong Zuo, Shujun Zhang **Copy Editor:** Fangling Lan **Production Editor:** Fangling Lan

## Abstract

Dielectric capacitors with ultrafast charge-discharge rates are extensively used in electrical and electronic systems. To meet the growing demand for energy storage applications, researchers have devoted significant attention to dielectric ceramics with excellent energy storage properties. As a result, the awareness of the importance of the pulsed discharge behavior of dielectric ceramics and conducting characterization studies has been raised. However, the temperature stability of pulsed discharge behavior, which is significant for pulsed power applications, is still not given the necessary consideration. Here, we systematically investigate the microstructures, energy storage properties and discharge behaviors of nanograined (1-x)BaTiO<sub>3</sub>-xNaNbO<sub>3</sub> ceramics prepared by a two-step sintering method. The 0.60BaTiO<sub>3</sub>-0.40NaNbO<sub>3</sub> ceramics with relaxor ferroelectric characteristics possess an optimal discharge energy density of 3.07 J cm<sup>-3</sup>, a high energy efficiency of 92.6%, an ultrafast discharge rate of 39 ns and a high power density of 100 MW cm<sup>-3</sup>. In addition to stable energy storage properties in terms of frequency, fatigue and temperature, the 0.60BaTiO<sub>3</sub>-0.40NaNbO<sub>3</sub> ceramics exhibit temperature-stable power density, thereby illustrating their significant potential for power electronics and pulsed power applications.

**Keywords:** BaTiO<sub>3</sub>-NaNbO<sub>3</sub>, energy storage properties, charge-discharge rate, temperature-stable power density



© The Author(s) 2023. **Open Access** This article is licensed under a Creative Commons Attribution 4.0 International License (<https://creativecommons.org/licenses/by/4.0/>), which permits unrestricted use, sharing, adaptation, distribution and reproduction in any medium or format, for any purpose, even commercially, as long as you give appropriate credit to the original author(s) and the source, provide a link to the Creative Commons license, and indicate if changes were made.



## INTRODUCTION

Dielectric capacitors, as fundamental components in high-power energy storage and pulsed power systems, play an important role in many applications, including hybrid electric vehicles, portable electronics, medical devices and electromagnetic weapons, due to their high power density, ultrafast charge-discharge rates and long lifetimes<sup>[1-6]</sup>. However, most current commercial polymer dielectric capacitors and multilayer ceramic capacitors (MLCCs) possess somewhat low energy densities of  $< 1\text{-}2 \text{ J cm}^{-3}$ , which results in them occupying relatively large volumes and/or weights in devices<sup>[7-10]</sup>. The development of third-generation semiconductors and the need for device miniaturization have resulted in an urgent demand for high-energy-density dielectric capacitors<sup>[1,11]</sup>.

Under an applied voltage, the dielectric materials in dielectric capacitors polarize to store energy<sup>[1,12,13]</sup>. Their energy storage properties can be calculated through polarization-electric field ( $P$ - $E$ ) loops, namely,  $W_c = \int_0^{P_{\max}} E dP$ ,  $W_d = \int_{P_r}^{P_{\max}} E dP$  and  $\eta = W_d/W_c$ , where  $W_c$  and  $W_d$  are the charge and discharge energy density, respectively,  $P_{\max}$  and  $P_r$  are the maximum and remnant polarization, respectively, and  $\eta$  is the energy efficiency<sup>[14-16]</sup>. Among all dielectric materials, relaxor ferroelectrics with high  $P_{\max}$ , low  $P_r$ , high breakdown strength ( $E_b$ ) and slim  $P$ - $E$  loops have been investigated extensively for their excellent energy storage properties<sup>[17-22]</sup>. The polar nanoregions in relaxor ferroelectrics can switch rapidly under an applied electric field, which significantly reduces loss and results in high  $\eta$ <sup>[23-28]</sup>. In addition, the excellent fatigue and temperature stability of the pulsed discharge behavior and energy storage properties are highly desirable for dielectric capacitors operating in harsh environments, i.e., aerospace fields and oil-well drilling<sup>[29-32]</sup>. Many strategies have been utilized to enhance the temperature stability of dielectric materials in recent years, including multiscale optimization<sup>[27]</sup>, composite strategy design<sup>[28]</sup>, unmatched temperature range design<sup>[33]</sup> and special sintering methods<sup>[34]</sup>. However, the temperature stability of pulsed discharge behavior is not given sufficient attention in current research into dielectric materials.

In this study, we prepare nanograined  $(1-x)\text{BaTiO}_3$ - $x\text{NaNbO}_3$  ceramics, which possess relaxor ferroelectric characteristics with a good  $P$ - $E$  relationship (high  $P_{\max}$ , low  $P_r$  and slim  $P$ - $E$  loops) and high  $E_b$ , using a solid-state reaction method. The  $0.60\text{BaTiO}_3$ - $0.40\text{NaNbO}_3$  ceramics exhibit an optimal  $W_d$  of  $3.07 \text{ J cm}^{-3}$  and a high  $\eta$  of 92.6% under  $38.1 \text{ MV m}^{-1}$  at ambient temperature. Stable energy storage properties in terms of frequency (0.1-100 Hz), fatigue ( $10^6$  cycles) and temperature (25-120 °C) are also achieved. Moreover, the ceramics possess an ultrafast discharge rate of 39 ns and a high power density of  $100 \text{ MW cm}^{-3}$ . The variation of the power density is less than 15% from 25 to 140 °C. All these results suggest that  $0.60\text{BaTiO}_3$ - $0.40\text{NaNbO}_3$  ceramics are ideal candidates for energy storage applications in pulsed power systems.

## MATERIALS AND METHODS

$(1-x)\text{BaTiO}_3$ - $x\text{NaNbO}_3$  ( $(1-x)\text{BT}$ - $x\text{NN}$ ) dielectric ceramics with  $x = 0.35, 0.40, 0.45$  and  $0.50$  were prepared through a conventional solid-state method. According to the stoichiometric ratio of  $(1-x)\text{BT}$ - $x\text{NN}$  ceramics,  $\text{BaCO}_3$ ,  $\text{TiO}_2$ ,  $\text{Na}_2\text{CO}_3$  and  $\text{Nb}_2\text{O}_5$  powders with analytical grade, as the raw materials, were weighed and ball milled with ethanol for 24 h. The mixed powders were then dried at 80 °C and calcined at 950-1030 °C for 5 h in the closed alumina crucibles to avoid the volatilization of Na. Afterward, the calcined  $(1-x)\text{BT}$ - $x\text{NN}$  powders were ground with a polyvinyl butyraldehyde solution (PVB, 10 wt.%) and uniaxially pressed into cylinders with a diameter of 8 mm and a thickness of 0.5 mm under a pressure of 2 MPa. The cylinders were heated at 600 °C for 5 h to remove the PVB binder and then sintered with a two-step sintering method<sup>[35,36]</sup> (all samples were heated to 1250-1350 °C for 1-10 min and then cooled down to 1100-1150 °C for 3-5 h).

The ambient-temperature X-ray diffraction profiles of the (1-*x*)BT-*x*NN ceramics were obtained using a Rigaku 2500 X-ray diffractometer (Rigaku, Tokyo, Japan) with Cu K $\alpha$  radiation and  $\lambda = 1.5418 \text{ \AA}$ . The surface microstructures of the ceramics after thermally etching at 1050 °C for 0.5 h were characterized using scanning electron microscopy (SEM, MERLIN VP Compact, Zeiss Ltd., Germany) at 15 kV. To measure the ferroelectric properties and pulsed discharge behaviors, the compact ceramics were polished down to 180-200  $\mu\text{m}$  in thickness and then gold electrodes with a radius of 1.5 mm were sputtered on both surfaces. The *P-E* loops were measured using a TF ANALYZER 2000E ferroelectric measurement system (aixACCT Systems GmbH, Aachen, Germany) under different frequencies (0.1-100 Hz) and various temperatures (25-140 °C). The dielectric properties were measured under a frequency range of 1 kHz to 1 MHz and a temperature range of -150 to 300 °C using an impedance analyzer (E4980A, Agilent Technologies, USA). The overdamped and underdamped pulsed discharge behavior was measured using a charge-discharge platform (CFD-001, Gogo Instruments Technology, Shanghai, China) with a resistor-capacitance load circuit. More details regarding the resistor-capacitance circuit measurement system are given in [Supplementary Figure 1](#).

## RESULTS AND DISCUSSION

The ambient-temperature X-ray diffraction profiles of the (1-*x*)BT-*x*NN ceramics are displayed in [Figure 1](#). All samples exhibit typical perovskite structures with traces of a Ba<sub>6</sub>Ti<sub>7</sub>Nb<sub>9</sub>O<sub>42</sub> secondary phase (PDF#47-0522). The approximate amounts of Ba<sub>6</sub>Ti<sub>7</sub>Nb<sub>9</sub>O<sub>42</sub> phases are displayed in [Supplementary Table 1](#) and are less than 5% in all (1-*x*)BT-*x*NN ceramics. The (200) peaks between 45° and 46° without splitting suggest that all samples are mainly pseudocubic phases at room temperature. The cell parameters of (1-*x*)BT-*x*NN ceramics decrease with increasing NN content [[Supplementary Table 2](#)], which is mainly because the radius of Na<sup>+</sup> (1.39 Å) is smaller than that of Ba<sup>2+</sup> (1.61 Å). The SEM images of the surface and cross-section microstructures of the (1-*x*)BT-*x*NN ceramics are displayed in [Figure 2](#) and [Supplementary Figure 2](#). There are no obvious pores in the (1-*x*)BT-*x*NN ceramics, suggesting that all samples possess high relative density. The grain size distributions [[Supplementary Figure 3](#)] are counted by the Feret diameters of more than 250 grains from the SEM images, and they show that all the ceramics possess nanograins with average grain sizes of 180-280 nm. The grain size tends to increase with NN content and the distribution moves toward larger sizes. Generally, fine grains are conducive to achieving high  $E_b$  and  $\eta$ . The elemental distribution results of the 0.60BT-0.40NN ceramics are shown in [Supplementary Figure 4](#), where it can be seen that all the elements are uniformly distributed in the ceramics.

The temperature-dependent (150-300 °C) dielectric properties of the (1-*x*)BT-*x*NN ceramics were measured at various frequencies [[Figure 3](#)] and indicated prototypical relaxor ferroelectric characteristics. The dielectric constants of all the (1-*x*)BT-*x*NN ceramics at room temperature are ~1000-1200 and the Ba<sub>6</sub>Ti<sub>7</sub>Nb<sub>9</sub>O<sub>42</sub> phases are considered to have paraelectric characteristics. Hence, the Ba<sub>6</sub>Ti<sub>7</sub>Nb<sub>9</sub>O<sub>42</sub> phases may not significantly affect the dielectric characteristics of the ceramics. It can be found that the dielectric constant and the Curie temperature increase with increasing NN content. All the (1-*x*)BT-*x*NN ceramics exhibit low dielectric loss of less than 0.012 between -100 and 200 °C. Generally, the modified Curie-Weiss law,  $1/\epsilon - 1/\epsilon_m = (T - T_m)^\gamma/C$ , is utilized to describe the dielectric characteristics of relaxor ferroelectrics, where  $\epsilon$  and  $\epsilon_m$  are the dielectric constant and maximum value of  $\epsilon$ , respectively,  $T$  and  $T_m$  are the corresponding temperatures,  $C$  is the Curie constant and  $\gamma$  is used to describe the degree of diffuseness. The  $\gamma$  value varies from one for typical ferroelectrics to two for ideal relaxor ferroelectrics<sup>[24,37]</sup>. The fitted  $\gamma$  values of all the ceramics are shown in [Figure 4](#) and are between 1.686 and 1.766 at 1 MHz, thereby manifesting strong relaxation behavior. This strong relaxation behavior causes the (1-*x*)BT-*x*NN ceramics to respond rapidly under an applied electric field, resulting in high  $\eta$ .

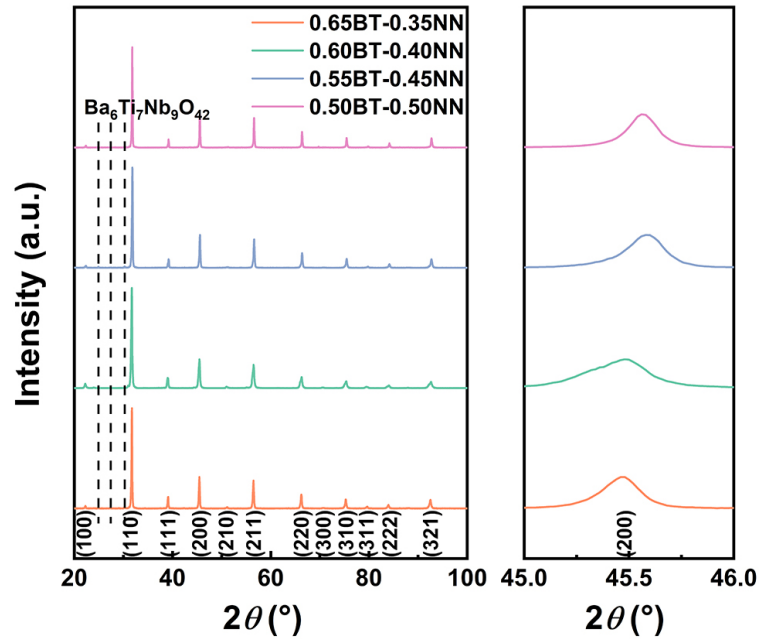


Figure 1. X-ray diffraction profiles of (1-x)BT-xNN ceramics.

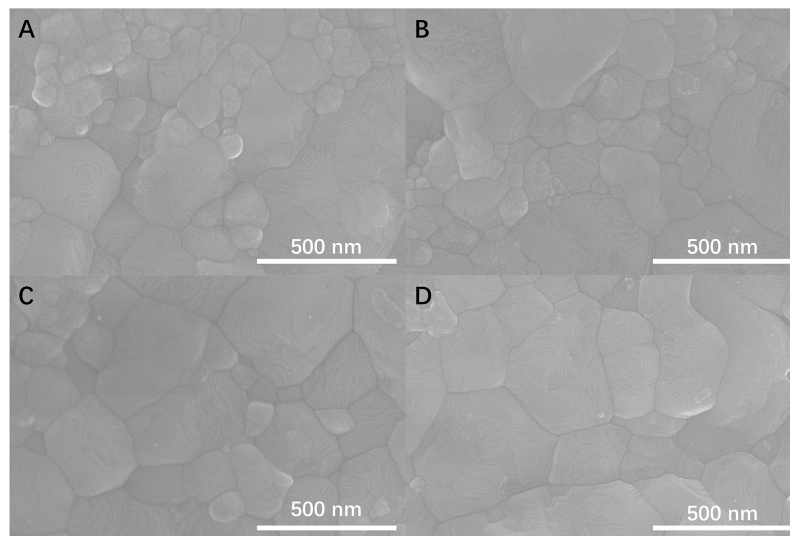
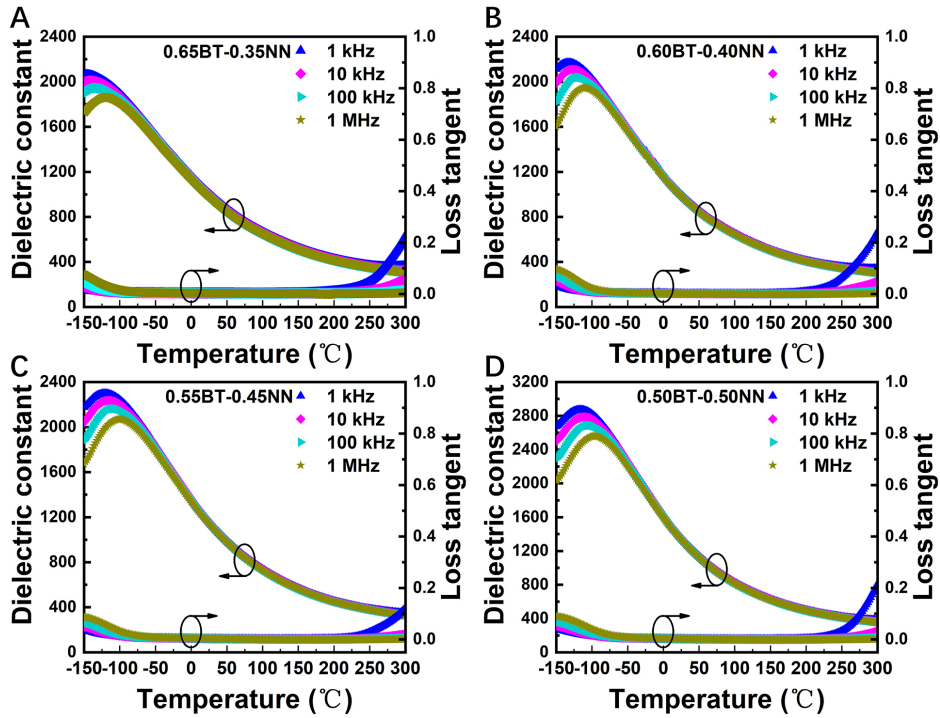
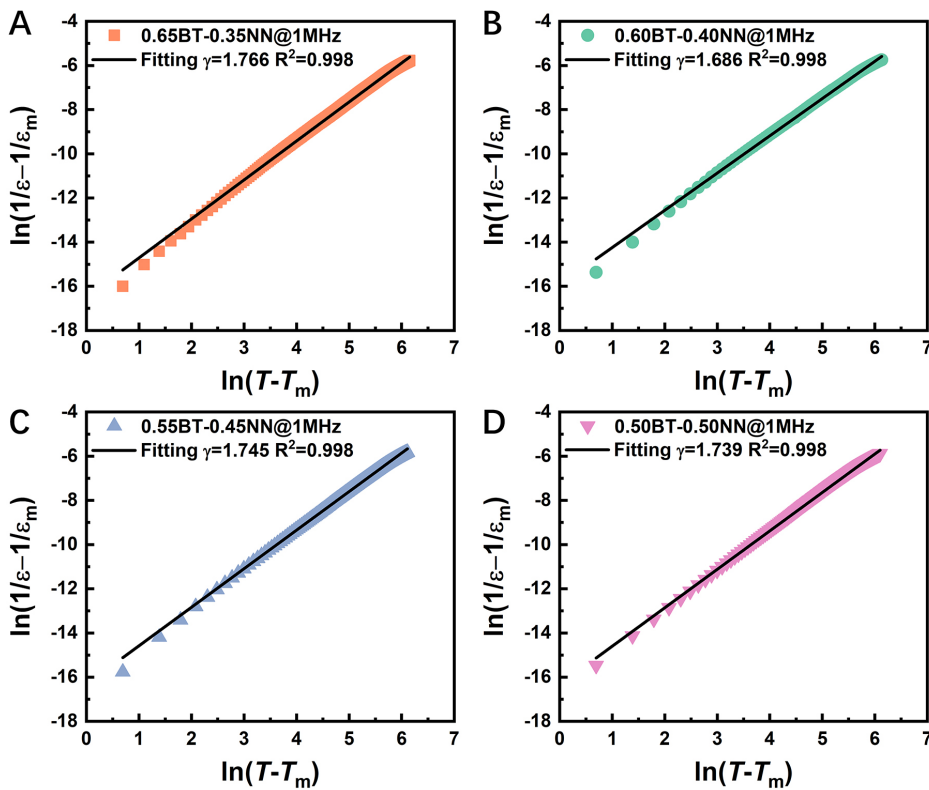


Figure 2. Surface microstructure images of (A) 0.65BT-0.35NN; (B) 0.60BT-0.40NN; (C) 0.55BT-0.45NN; and (D) 0.50BT-0.50NN.

The unipolar  $P$ - $E$  loops of all ceramics measured at 25 °C and 20 MV m<sup>-1</sup> are shown in Figure 5A, with all ceramics exhibiting slim  $P$ - $E$  loops. Among these, the 0.55BT-0.45NN ceramics possess the largest  $P_{\max}$  and  $P_{\max} - P_r$  values [Figure 5B], leading to high  $W_d$ . However, due to the lower  $P_r$ , relatively larger  $P_{\max} - P_r$  value and the highest  $E_b$  [Figure 5B and C], a  $W_d$  of 3.07 J cm<sup>-3</sup> and a high  $\eta$  of 92.6% are achieved in the 0.60BT-0.40NN ceramics at 38.1 MV m<sup>-1</sup>, which are the optimum energy storage properties among all the (1-x)BT-xNN ceramics at 25 °C [Figure 5D]. Figure 6 exhibits the energy storage properties as a function of the applied electric field. All BT-NN ceramics possess high  $E_b$  between 32.7 and 38.1 MV m<sup>-1</sup> and high  $\eta$  between 87.5% and 93.0%. The corresponding current-field curves of the (1-x)BT-xNN ceramics are shown



**Figure 3.** Temperature-dependent dielectric properties measured at 1 kHz to 1 MHz for (A) 0.65BT-0.35NN; (B) 0.60BT-0.40NN; (C) 0.55BT-0.45NN; and (D) 0.50BT-0.50NN.



**Figure 4.** Fitted  $\gamma$  values for (A) 0.65BT-0.35NN; (B) 0.60BT-0.40NN; (C) 0.55BT-0.45NN; and (D) 0.50BT-0.50NN.

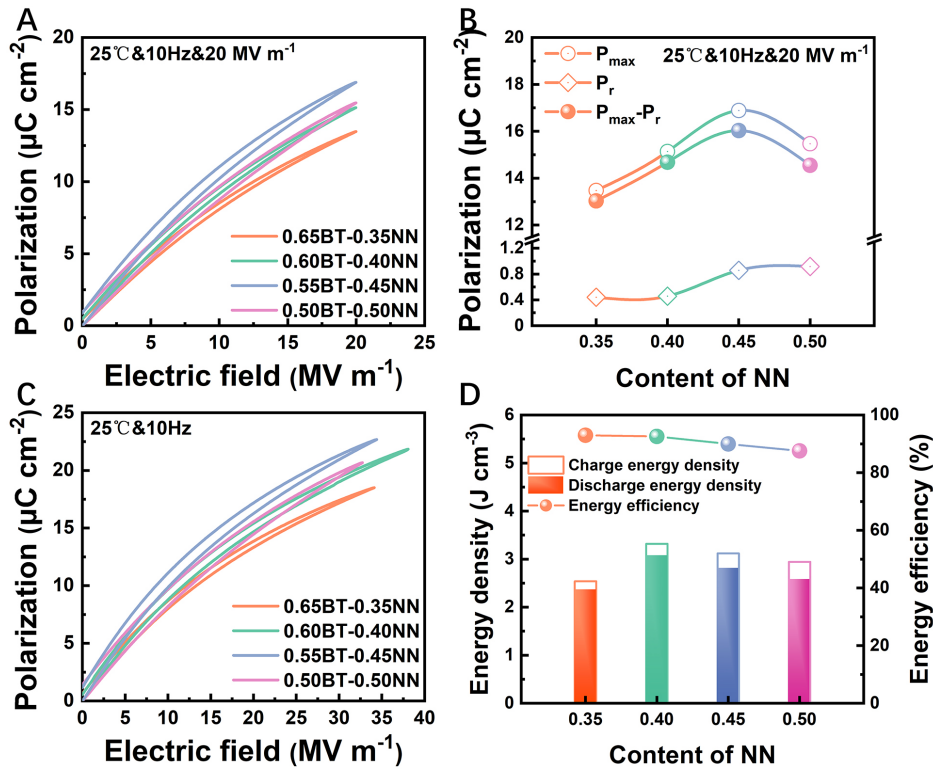


**Figure 5.** (A) Unipolar  $P$ - $E$  loops for  $(1-x)\text{BT}-x\text{NN}$  ceramics at  $25\text{ }^{\circ}\text{C}$ ,  $20\text{ MV m}^{-1}$  and  $10\text{ Hz}$ . (B)  $P_{\text{max}}$ ,  $P_r$ , and  $P_{\text{max}} - P_r$  as a function of NN content. (C) Unipolar  $P$ - $E$  loops at  $25\text{ }^{\circ}\text{C}$ , maximum applied electric field and  $10\text{ Hz}$ . (D) Energy storage properties as a function of NN content.

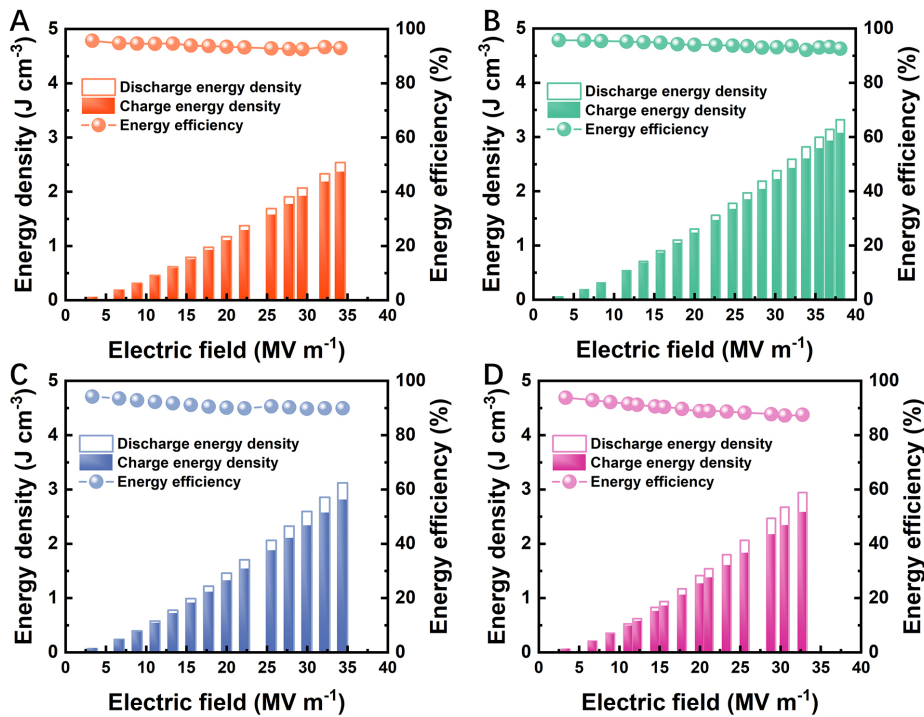


**Figure 6.** Energy storage properties at  $25\text{ }^{\circ}\text{C}$  and  $10\text{ Hz}$  for (A) 0.65BT-0.35NN; (B) 0.60BT-0.40NN; (C) 0.55BT-0.45NN; and (D) 0.50BT-0.50NN.

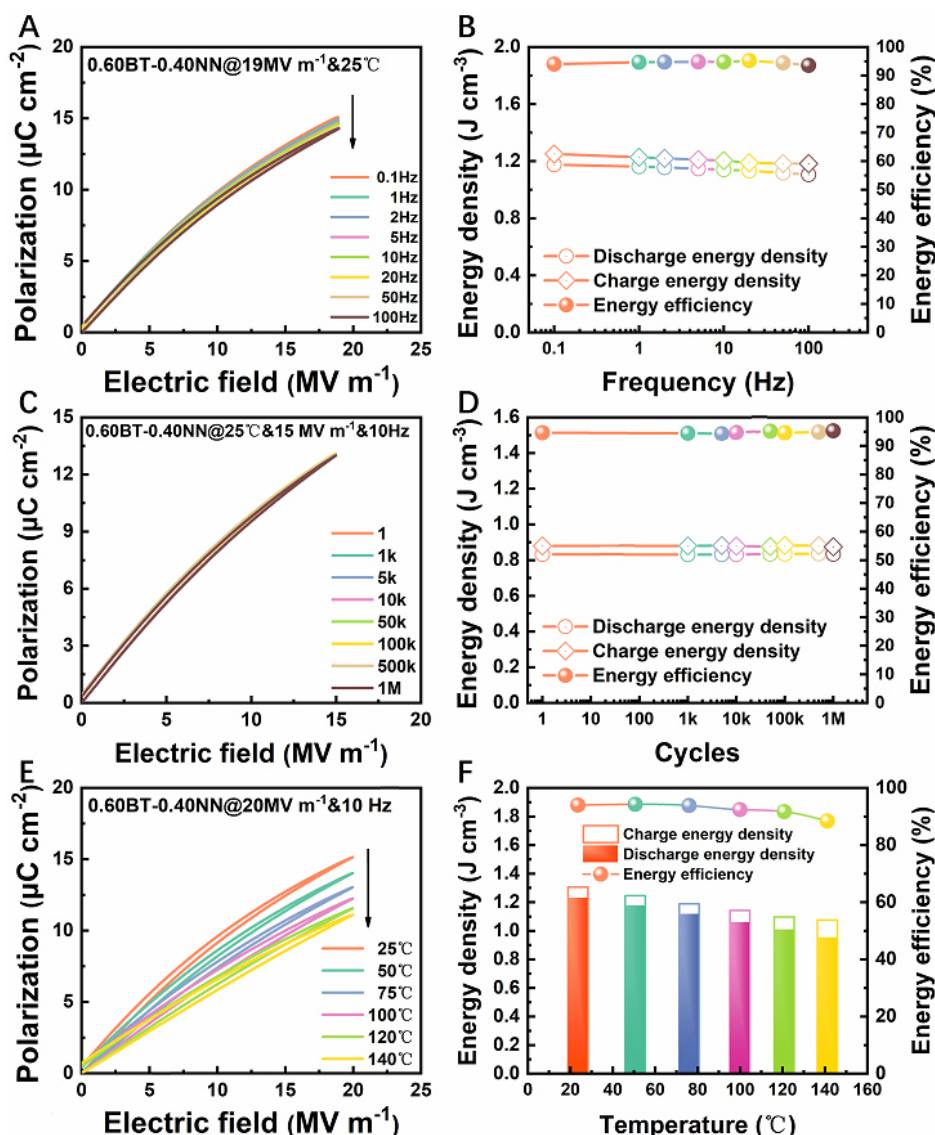


**Figure 7.** (A) Unipolar  $P$ - $E$  loops of 0.60BT-0.40NN ceramics measured under  $19 \text{ MV m}^{-1}$  at various frequencies, (C) under  $15 \text{ MV m}^{-1}$  at different cycles and (E) under  $20 \text{ MV m}^{-1}$  at various temperatures. Corresponding (B) frequency-dependent, (D) fatigue-dependent and (F) temperature-dependent energy storage properties.

in [Supplementary Figure 5](#), confirming the high  $\eta$ . Noticeably, the  $\eta$  of the 0.60BT-0.40NN ceramics decreases slightly with increasing  $E$  and shows a slight variation of  $< 4\%$  within the whole electric field range tested, which is conducive to high  $\eta$  energy storage applications.

Given that the stability of the energy storage properties for dielectric materials is crucial in practical applications, the frequency, fatigue and temperature stabilities of the energy storage properties for the 0.60BT-0.40NN ceramics are characterized in [Figure 7](#). The  $P_{\text{max}}$  of the 0.60BT-0.40NN ceramics only decreases from  $15.1$  to  $14.3 \mu\text{C cm}^{-2}$  with increasing frequency from  $0.1$  to  $100 \text{ Hz}$ , while the  $P_r$  remains almost unchanged [[Figure 7A](#)]. Hence, the variations in  $W_d$  and  $\eta$  are less than  $6.0\%$  and  $1.2\%$ , respectively [[Figure 7B](#)]. The stable frequency-dependent energy storage properties are realized because the polar nanoregions can switch rapidly under the applied electric field<sup>[38]</sup>. To evaluate the fatigue stability, the unipolar  $P$ - $E$  loops under  $15 \text{ MV m}^{-1}$  are characterized for  $10^6$  cycles [[Figure 7C](#)]. Fortunately, the  $P$ - $E$  loops

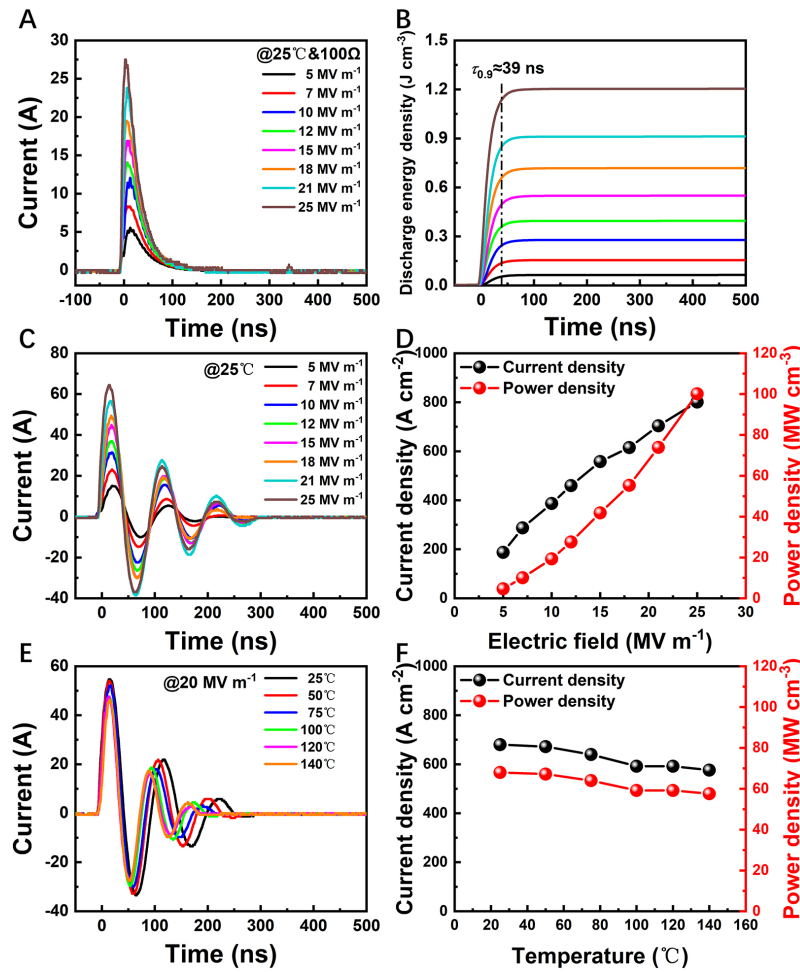


**Figure 8.** (A) Overdamped pulsed discharge current curves under various  $E$  values and (B) corresponding  $W_d$  as a function of time. Undamped pulsed discharge current curves (C) at 25 °C under various  $E$  values and (E) at 20 MV m<sup>-1</sup> under various temperatures and (D and F) corresponding  $C_D$  and  $P_D$  values.

have no noticeable change and the variations in  $W_d$  and  $\eta$  are less than 0.6% and 0.7%, respectively [Figure 7D]. Figure 7E exhibits the unipolar  $P$ - $E$  loops measured under 20 MV m<sup>-1</sup> at various temperatures. It can be found that the  $P_{\max}$  of the 0.60BT-0.40NN ceramics is consistent with the trend of the  $\epsilon$  and gradually decreases with increasing temperature. The reduction in  $P_{\max}$  results in a decrease in  $W_d$ , while the  $\eta$  stays over 90% when the temperature is up to 120 °C. Figure 7F shows the energy storage properties ( $W_d$  and  $\eta$ ) of the 0.60BT-0.40NN ceramics with increasing temperature from 25 to 120 °C, revealing good temperature stability.

In practical applications, dielectric capacitors charge and discharge at the microsecond or nanosecond timescale<sup>[1]</sup>. The  $W_d$  and  $\eta$  calculated by the  $P$ - $E$  loops cannot reflect the true energy storage properties<sup>[39]</sup>, so a resistor-capacitance circuit is constructed to evaluate the discharge behavior of the 0.60BT-0.40NN ceramics. Figure 8A displays the overdamped pulsed discharge electric current-time ( $I$ - $t$ ) curves at various  $E$  values. The corresponding  $W_d$  can be calculated using  $W_d = \int I(t)^2 R dt / V$ , where  $R$  and  $V$  are the load resistor (here  $R = 100 \Omega$ ) and the effective volume of the sample, respectively<sup>[40]</sup>. The discharge rate is usually described by the discharge time corresponding to the 90% stored  $W_d$  value, which is abbreviated as  $\tau_{0.9}$ . As the  $E$  increases, the current peak and  $W_d$  also increase. Finally, the  $W_d$  reaches 1.21 J cm<sup>-3</sup> at 25 MV m<sup>-1</sup>

[Figure 8B]. In general, the  $W_d$  calculated by the  $I-t$  curve is always lower than that calculated by the  $P-E$  loop because the characterization mechanisms with different measurement frequencies<sup>[1]</sup> and dielectric material losses differ<sup>[41]</sup>. The  $\tau_{0.9}$  of the 0.60BT-0.40NN ceramics is  $\sim 39$  ns [Figure 8B]. The ultrafast discharge rate comes from the low hysteresis polarization response and the relaxor characteristic. This makes the 0.60BT-0.40NN ceramics more competitive in high-power applications<sup>[38,42]</sup>. Moreover, the undamped pulsed discharge current curves at 25 °C under various  $E$  values are displayed in Figure 8C. From the current curves, we can calculate the current density ( $C_D$ ) and power density ( $P_D$ ) from  $C_D = I_{\max}/S$  and  $P_D = EI_{\max}/2S$ , where  $I_{\max}$  and  $S$  represent the maximum value of the undamped pulsed discharge current curves and the electrode area, respectively<sup>[26]</sup>. The  $C_D$  and  $P_D$  of the 0.60BT-0.40NN ceramics at 25 MV m<sup>-1</sup> are 801 A cm<sup>-2</sup> and 100 MW cm<sup>-3</sup>, respectively [Figure 8D]. More importantly, from the undamped pulsed discharge current curves at 20 MV m<sup>-1</sup> under various temperatures [Figure 8E], it can be found that the variations of  $C_D$  and  $P_D$  are  $\sim 15\%$  from 25 to 140 °C [Figure 8F], which suggests that the 0.60BT-0.40NN ceramics have significant potential for pulsed power system applications.

## CONCLUSIONS

In summary, the 0.60BT-0.40NN ceramics with relaxor ferroelectric characteristics have an optimal  $W_d$  of 3.07 J cm<sup>-3</sup>, a high  $\eta$  of 92.6%, a high  $P_D$  of 100 MW cm<sup>-3</sup> and an ultrafast  $\tau_{0.9}$  of 39 ns. Moreover, they exhibit stable energy storage properties in terms of frequency (0.1-100 Hz), fatigue ( $10^6$  cycles) and temperature (25-120 °C), as well as temperature-stable power density (25-140 °C). These ideal energy storage properties and pulsed discharge behavior make the 0.60BT-0.40NN ceramics more promising for high-stability energy storage MLCCs in pulsed power system applications.

## DECLARATIONS

### Author's contributions

Sample fabrication and characterization: Zhao P

Data analysis and interpretation: Li L, Wang X

Preparation of the manuscript and discussion: Zhao P, Li L, Wang X

### Availability of data and materials

Data can be deposited into data repositories or published as supplementary information in the journal.

### Financial support and sponsorship

This work was supported by Shuimu Tsinghua Scholar Program, Key-Area Research and Development Program of Guangdong Province (No. 2019B090912003), National Natural Science Foundation of China (No. 52032005), High-end MLCC Key Project Supported by Guangdong Fenghua Advanced Technology Holding Co., Ltd.

### Conflicts of interest

All authors declared that there are no conflicts of interest.

### Ethical approval and consent to participate

Not applicable.

### Consent for publication

Not applicable.

## Copyright

© The Author(s) 2023.

## REFERENCES

1. Zhao P, Cai Z, Wu L, et al. Perspectives and challenges for lead-free energy-storage multilayer ceramic capacitors. *J Adv Ceram* 2021;10:1153-93. DOI
2. Wang G, Lu Z, Li Y, et al. Electroceramics for high-energy density capacitors: current status and future perspectives. *Chem Rev* 2021;121:6124-72. DOI PubMed PMC
3. Palneedi H, Peddigari M, Hwang G-T, Jeong D-Y, Ryu J. High-performance dielectric ceramic films for energy storage capacitors: progress and outlook. *Adv Funct Mater* 2018;28:1803665. DOI
4. Li Q, Chen L, Gadinski MR, et al. Flexible high-temperature dielectric materials from polymer nanocomposites. *Nature* 2015;523:576-9. DOI PubMed
5. Whittingham MS. Materials challenges facing electrical energy storage. *MRS Bull* 2008;33:411-9. DOI
6. Li J, Shen Z, Chen X, et al. Grain-orientation-engineered multilayer ceramic capacitors for energy storage applications. *Nat Mater* 2020;19:999-1005. DOI PubMed
7. Xu R, Feng Y, Wei X, Xu Z. Analysis on nonlinearity of antiferroelectric multilayer ceramic capacitor (MLCC) for energy storage. *IEEE Trans Dielect Electr Insul* 2019;26:2005-11. DOI
8. Love GR. Energy storage in ceramic dielectrics. *J Am Ceram Soc* 1990;73:323-8. DOI
9. Jow TR, MacDougall FW, Ennis JB, et al. Pulsed power capacitor development and outlook. In 2015 IEEE Pulsed Power Conference (PPC); 2015, pp. 1-7. DOI
10. Wang Y, Zhou X, Chen Q, Chu BJ, Zhang QM. Recent development of high energy density polymers for dielectric capacitors. *IEEE Trans Dielect Electr Insul* 2010;17:1036-42. DOI
11. Kim J, Saremi S, Acharya M, et al. Ultrahigh capacitive energy density in ion-bombarded relaxor ferroelectric films. *Science* 2020;369:81-4. DOI PubMed
12. Liu Z, Lu T, Ye J, et al. Antiferroelectrics for energy storage applications: a review. *Adv Mater Technol* 2018;3:1800111. DOI
13. Hong K, Lee TH, Suh JM, Yoon S-H, Jang HW. Perspectives and challenges in multilayer ceramic capacitors for next generation electronics. *J Mater Chem C* 2019;7:9782-802. DOI
14. Li F, Zhai J, Shen B, Zeng H. Recent progress of ecofriendly perovskite-type dielectric ceramics for energy storage applications. *J Adv Dielect* 2019;8:1830005. DOI
15. Zhang H, Wei T, Zhang Q, et al. A review on the development of lead-free ferroelectric energy-storage ceramics and multilayer capacitors. *J Mater Chem C* 2020;8:16648-67. DOI
16. Yao Z, Song Z, Hao H, et al. Homogeneous/inhomogeneous-structured dielectrics and their energy-storage performances. *Adv Mater* 2017;29:1601727. DOI PubMed
17. Ogihara H, Randall CA, Trolrier-McKinstry S. High-energy density capacitors utilizing 0.7BaTiO<sub>3</sub>-0.3BiScO<sub>3</sub> ceramics. *J Am Ceram Soc* 2009;92:1719-24. DOI
18. Wang Z, Kang R, Liu W, et al. (Bi<sub>0.5</sub>Na<sub>0.5</sub>)TiO<sub>3</sub>-based relaxor ferroelectrics with medium permittivity featuring enhanced energy-storage density and excellent thermal stability. *Chem Eng J* 2022:427. DOI
19. Yang L, Kong X, Cheng Z, Zhang S. Ultra-high energy storage performance with mitigated polarization saturation in lead-free relaxors. *J Mater Chem A* 2019;7:8573-80. DOI
20. Yang L, Kong X, Cheng Z, Zhang S. Enhanced energy density and electric cycling reliability via MnO<sub>2</sub> modification in sodium niobate-based relaxor dielectric capacitors. *J Mater Res* ;2021, 36:1214-1222. DOI
21. Wang X, Huan Y, Zhao P, et al. Optimizing the grain size and grain boundary morphology of (K,Na)NbO<sub>3</sub>-based ceramics: Paving the way for ultrahigh energy storage capacitors. *J Mater* 2021;7:780-9. DOI
22. Zhao P, Wang H, Wu L, et al. High-performance relaxor ferroelectric materials for energy storage applications. *Adv Energy Mater* 2019;9:1803048. DOI
23. Pan H, Li F, Liu Y, et al. Ultrahigh-energy density lead-free dielectric films via polymorphic nanodomain design. *Science* 2019;365:578-82. DOI PubMed
24. Yuan Q, Li G, Yao F-Z, et al. Simultaneously achieved temperature-insensitive high energy density and efficiency in domain engineered BaTiO<sub>3</sub>-Bi(Mg<sub>0.5</sub>Zr<sub>0.5</sub>)O<sub>3</sub> lead-free relaxor ferroelectrics. *Nano Energy* 2018;52:203-10. DOI
25. Wu L, Wang X, Li L. Lead-free BaTiO<sub>3</sub>-Bi(Zn<sub>2/3</sub>Nb<sub>1/3</sub>)O<sub>3</sub> weakly coupled relaxor ferroelectric materials for energy storage. *RSC Adv* 2016;6:14273-82. DOI
26. Zhou M, Liang R, Zhou Z, Dong X. Superior energy storage properties and excellent stability of novel NaNbO<sub>3</sub>-based lead-free ceramics with A-site vacancy obtained via a Bi<sub>2</sub>O<sub>3</sub> substitution strategy. *J Mater Chem A* 2018;6:17896-904. DOI
27. Zhao P, Cai Z, Chen L, et al. Ultra-high energy storage performance in lead-free multilayer ceramic capacitors via a multiscale optimization strategy. *Energy Environ Sci* 2020;13:4882-90. DOI
28. Zhao P, Chen L, Li L, Wang X. Ultrahigh energy density with excellent thermal stability in lead-free multilayer ceramic capacitors via composite strategy design. *J Mater Chem A* 2021;9:25914-21. DOI
29. Chen L, Wang H, Zhao P, et al. Effect of MnO<sub>2</sub> on the dielectric properties of Nb-doped BaTiO<sub>3</sub>-(Bi<sub>0.5</sub>Na<sub>0.5</sub>)TiO<sub>3</sub> ceramics for X9R

- MLCC applications. *J Am Ceram Soc* 2018;102:2781-90. DOI
30. Hui K, Chen L, Cen Z, et al. KNN based high dielectric constant X9R ceramics with fine grain structure and energy storage ability. *J Am Ceram Soc* 2021;104:5815-25. DOI
  31. Li T, Qiao Z, Zuo R. X9R-type  $\text{Ag}_{1-3x}\text{Bi}_x\text{NbO}_3$  based lead-free dielectric ceramic capacitors with excellent energy-storage properties. *Ceram Int* 2022;48:2533-7. DOI
  32. Zhu C, Cai Z, Luo B, et al. High temperature lead-free BNT-based ceramics with stable energy storage and dielectric properties. *J Mater Chem A* 2020;8:683-92. DOI
  33. Yang Z, Du H, Jin L, et al. Realizing high comprehensive energy storage performance in lead-free bulk ceramics via designing an unmatched temperature range. *J Mater Chem A* 2019;7:27256-66. DOI
  34. Cai Z, Zhu C, Wang H, et al. High-temperature lead-free multilayer ceramic capacitors with ultrahigh energy density and efficiency fabricated via two-step sintering. *J Mater Chem A* 2019;7:14575-82. DOI
  35. Chen I-W, XH W. Sintering dense nanocrystalline ceramics without final-stage grain growth. *Nature* 2000;404:168. DOI PubMed
  36. Wang XH, Deng X-Y, Bai H-L, et al. Two-step sintering of ceramics with constant grain-size, II:  $\text{BaTiO}_3$  and Ni-Cu-Zn ferrite. *J Am Ceram Soc* 2006;89:438-43. DOI
  37. Shen Z, Wang X, Luo B, Li L.  $\text{BaTiO}_3$ - $\text{BiYbO}_3$  perovskite materials for energy storage applications. *J Mater Chem A* 2015;3:18146-53. DOI
  38. Zhu C, Cai Z, Guo L, et al. Simultaneously achieved ultrastable dielectric and energy storage properties in lead-free  $\text{Bi}_{0.5}\text{Na}_{0.5}\text{TiO}_3$ -based ceramics. *ACS Appl Energy Mater* 2022;5:1560-70. DOI
  39. Yang L, Kong X, Li F, et al. Perovskite lead-free dielectrics for energy storage applications. *Prog Mater Sci* 2019;102:72-108. DOI
  40. Hao X. A review on the dielectric materials for high energy-storage application. *J Adv Dielectr* 2013;03:1330001. DOI
  41. Li J, Li F, Xu Z, Zhang S. Multilayer lead-free ceramic capacitors with ultrahigh energy density and efficiency. *Adv Mater* 2018;30:1802155. DOI PubMed
  42. Yang D, Gao J, Shu L, et al. Lead-free antiferroelectric niobates  $\text{AgNbO}_3$  and  $\text{NaNbO}_3$  for energy storage applications. *J Mater Chem A* 2020;8:23724-37. DOI